



Lawrence Berkeley Laboratory

UNIVERSITY OF CALIFORNIA

Materials & Molecular Research Division

Submitted to the Journal of the Electrochemical Society

MATHEMATICAL MODELING OF THE LITHIUM-ALUMINUM, IRON
SULFIDE BATTERY. I. THE INFLUENCE OF RELAXATION TIME
ON THE CHARGING CHARACTERISTICS

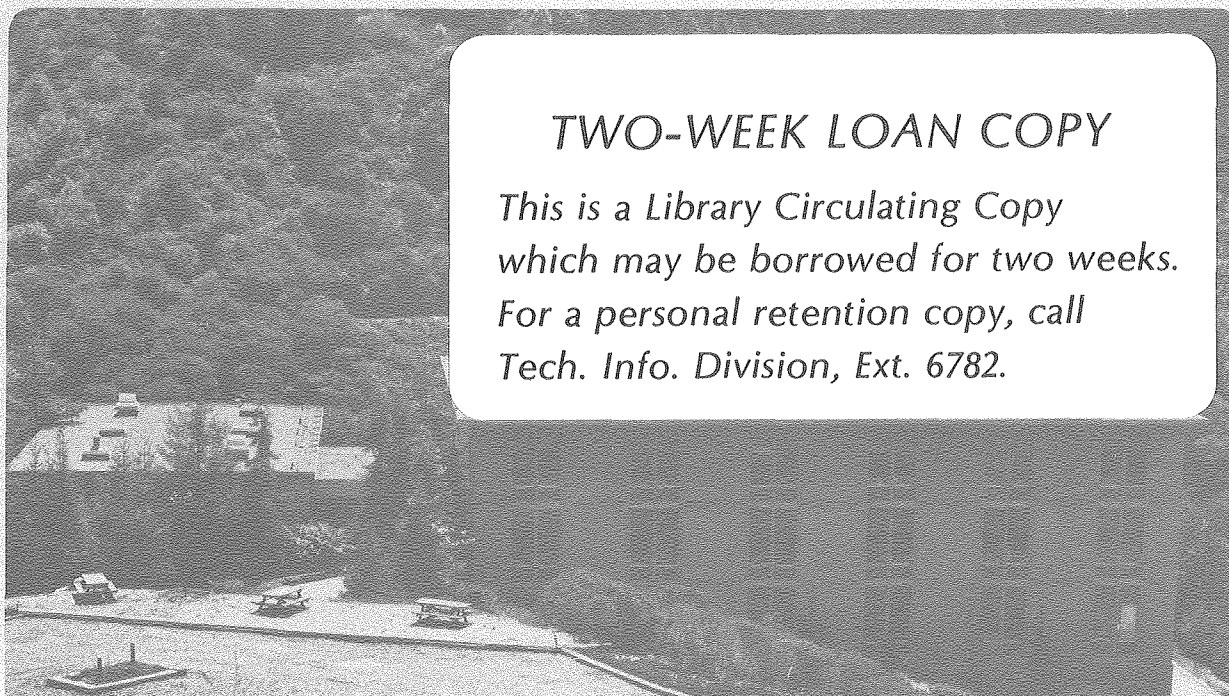
Richard Pollard and John Newman

January 1980

RECEIVED
LAWRENCE
BERKELEY LABORATORY

MAR 14 1980

LIBRARY AND
DOCUMENTS SECTION



TWO-WEEK LOAN COPY

*This is a Library Circulating Copy
which may be borrowed for two weeks.
For a personal retention copy, call
Tech. Info. Division, Ext. 6782.*

LBL 10421 c.2

DISCLAIMER

This document was prepared as an account of work sponsored by the United States Government. While this document is believed to contain correct information, neither the United States Government nor any agency thereof, nor the Regents of the University of California, nor any of their employees, makes any warranty, express or implied, or assumes any legal responsibility for the accuracy, completeness, or usefulness of any information, apparatus, product, or process disclosed, or represents that its use would not infringe privately owned rights. Reference herein to any specific commercial product, process, or service by its trade name, trademark, manufacturer, or otherwise, does not necessarily constitute or imply its endorsement, recommendation, or favoring by the United States Government or any agency thereof, or the Regents of the University of California. The views and opinions of authors expressed herein do not necessarily state or reflect those of the United States Government or any agency thereof or the Regents of the University of California.

Mathematical Modeling of the Lithium-Aluminum,
Iron Sulfide Battery

II. The Influence of Relaxation Time on the Charging
Characteristics

Richard Pollard^{*,1} and John Newman

Materials and Molecular Research Division, Lawrence Berkeley Laboratory
and Department of Chemical Engineering, University of California,
Berkeley, California 94720

January 1980

ABSTRACT

A mathematical model of the LiAl/LiCl, KCl/FeS cell has been used to study the behavior of the system during relaxation and charging. The effects of state of charge, cell temperature, and current density are presented, and the influence of a period of relaxation on the subsequent charging operation is investigated. In addition, factors that can have a significant impact on the charging characteristics are identified.

¹Present address: Department of Chemical Engineering, University of Houston, Houston, Texas 77004

* Electrochemical Society Active Member

Key words: porous electrodes, molten salt electrolyte, cell performance

Introduction

The mathematical model of the LiAl/LiCl, KCl/FeS cell¹ can also be used to investigate the behavior of the system during relaxation and charging. The changes that take place under these conditions could influence the dependence of cell performance on the number of completed cycles.

In the laboratory, current interruption techniques can be used to assess the resistance within the electrodes, separator, and grids. Furthermore, in some experiments, such as post-mortem cell examinations, a period of relaxation may be needed before the temperature is low enough to begin the analyses. Current interruption may also be important in modules for electric vehicle propulsion, where it is anticipated that there will be significant periods when the battery is not in use. Cell behavior on charge can control the overall energy efficiency of the system and may also directly affect the nature of the subsequent cell discharge.^{2,3} For these reasons, it is necessary to identify the factors that can limit the system during the relaxation and charging modes of operation.

The governing differential equations presented previously¹ can be used directly in the analysis, and it is only necessary to replace the initial conditions, $x_A = x_A^0$ and $\varepsilon = \varepsilon^0$, with the appropriate composition and porosity distributions and to modify the model for negative electrode kinetics. At any point in the electrode, it is assumed that an outer layer of β -LiAl forms as soon as charging begins, and that the electrochemical reaction is restricted to the solid-electrolyte interface.

The analysis of diffusion of lithium through the β -phase and the gradual reduction in thickness of the α -Al region parallels the model for discharge,^{1,4} but the limiting transfer current becomes

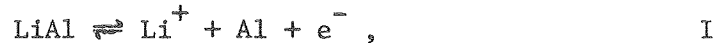
$$(V \cdot i_2)_{\text{lim}} = \frac{4\pi NFD_{\beta} (c_{\text{Li}}^{\beta})_{\text{sat}}}{(1-x_{\text{Li}}^{\beta}) \left(\frac{1}{r_0} - \frac{1}{r_1} \right)}, \quad (1)$$

and the reference concentration $(c_{\text{Li}}^{\alpha})_{\text{sat}}$ should be replaced by $(c_{\text{Li}}^{\beta})_{\text{sat}}$.

Results and Discussion

Relaxation

Figure 1 shows composition profiles across the cell sandwich for several times after interruption of the current at the end of a discharge with $I = 41.6 \text{ mA/cm}^2$. The concentration variations diminish in both electrodes and, after 2 hours, the electrolyte composition is practically uniform. In the negative, the region with highest x_A , at the back of the electrode, becomes cathodic with respect to the front portions. Local concentration cells, with the reaction

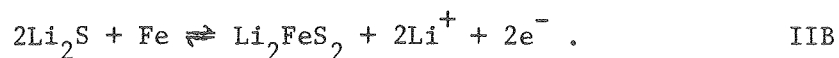


are established that reduce the initial composition variations. However, there is no driving force for equalization of the local state of charge within the α -Al, β -LiAl alloy, and the reactions that take place to give a uniform electrolyte composition accentuate the nonuniform utilization of reactants. The magnitude of this effect is dependent on the composition profile and the depth of discharge before current interruption.

In the positive electrode, the situation is complicated by the possibility of simultaneous reactions and by precipitation of electrolyte. Initially, the electrolyte concentration is almost uniform across the majority of the electrode due to precipitation of KCl as two spikes adjacent to the reaction fronts, and self-discharge reactions in the isolated regions behind the spikes. Adjacent to the current collector, FeS reacts with lithium ions according to

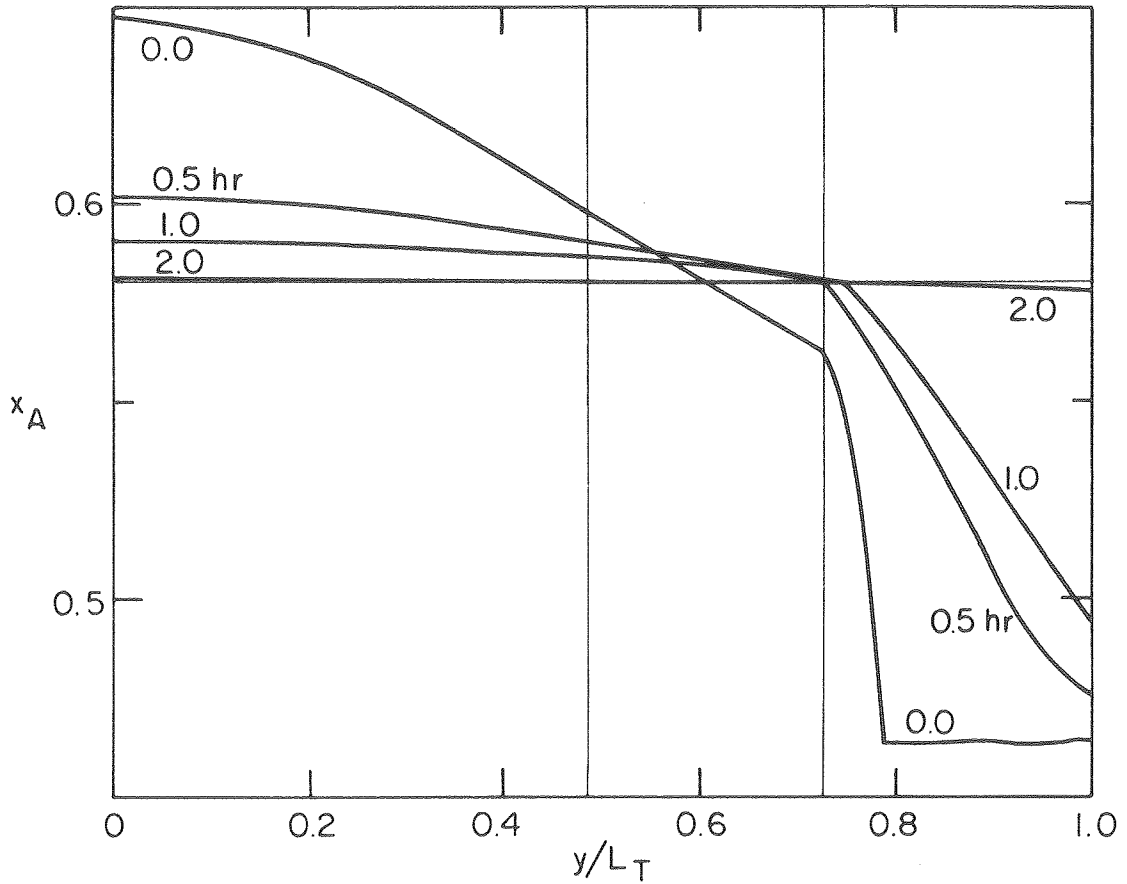


whereas, near the front of the electrode, Li_2S reacts anodically with iron, thus:



The transformation of Li_2S and FeS to the intermediate sulfide reduces the local variations in state of charge although, once all the FeS has been removed, it is not possible for the remainder of the Li_2S to react further. Consequently after approximately 1 hour, there are no more reactions in the positive, and the composition now relaxes under the influence of diffusion alone.

Characteristic times for other relaxation processes can also be identified from the composition profiles. In Fig. 1, the electrolyte concentration changes by less than 1% across the separator after 1.3 hours, whereas the 1% condition is achieved in the negative electrode after only 0.8 hours. This reflects, to some extent, the influence of the electrochemical reaction on the relaxation time.⁵ However, the 1% criterion



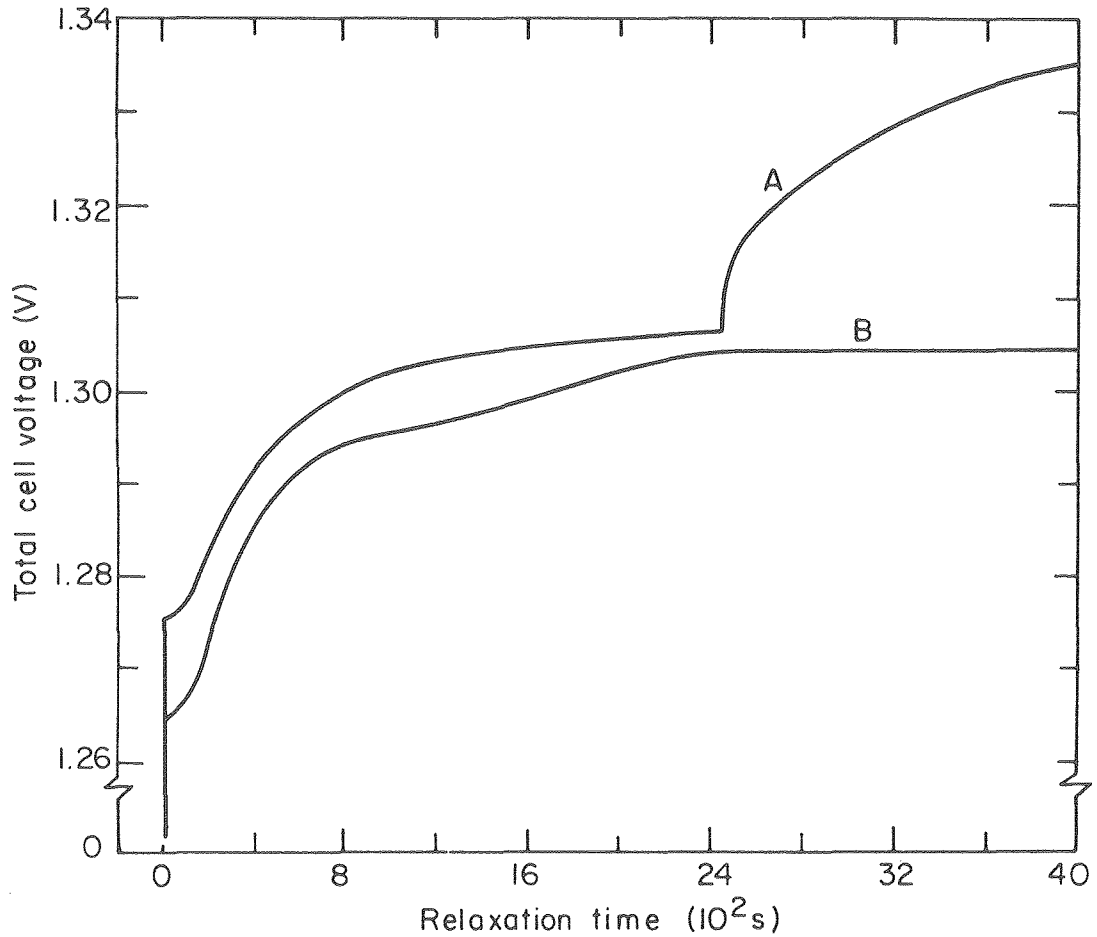
XBL 7912-14569

Fig. 1. Position dependence of mole fraction of LiCl at different times after current interruption. Simulation parameters: $Q_- = 2800 \text{ c/cm}^3$, $Q_+ = 4630 \text{ c/cm}^3$, $L_- = 0.32 \text{ cm}$, $L_s = 0.16 \text{ cm}$, $L_+ = 0.18 \text{ cm}$, $N = 5.5 \times 10^7 \text{ cm}^{-3}$, $h_o = 8.25 \times 10^{-2} \text{ W/m}^2 \cdot \text{K}$, $R_s = 1.55 \Omega \text{ cm}^2$, $h = 0.004 \text{ cm}$, $w = 0$, $-c_{\text{Li}}^{-\beta} / (c_{\text{Li}}^{\beta})_{\text{sat}} = 1.0$, $D_{\beta} = 4 \times 10^{-8} \text{ cm}^2/\text{s}$. Parameters at start of previous discharge: $\epsilon_-^o = 0.39$, $\epsilon_s = 0.75$, $\epsilon_+^o = 0.555$, $T_o = 470^\circ\text{C}$, $I = 41.6 \text{ mA/cm}^2$, $x_A^o = 0.58$. Initial stage of charge, $\lambda(t = 0) = 47.9\%$. Additional parameters specified in Tables 1 and 3 of Reference 1.

is rather arbitrary and, even though the composition is fairly uniform at 0.8 hours, the concentration in the negative still needs to drop by another 2.5%, as diffusion takes place across the separator. In the positive, an additional characteristic time can be distinguished. Self-discharge reactions take place in the region where Li_2FeS_2 is only partially converted to Li_2S . Here, the portion closest to the front of the electrode becomes preferentially cathodic and, after approximately 4 minutes, a sharp reaction front for the second reaction has been formed.

Heat is not generated in the cell during relaxation, and the temperature falls in accordance with the specified rate of heat transfer to the surroundings. As a result, the saturation concentration for KCl can rise faster than the minimum electrolyte concentration and, under these circumstances, the total volume of precipitate becomes greater than the value at current interruption. However, the reduction in minimum composition soon dominates and, in this example, all the KCl has dissolved after 1500 s.

Figure 2 shows the variations in total cell voltage that take place after the current is switched off, for simulations A and B described in Fig. 9 of Reference 1. Curve A is for the example that had a temperature of 450°C at the start of discharge, and that achieved 39.2% utilization before the cutoff voltage was reached. The second example had a higher initial temperature (470°C), and a greater utilization was attained before the termination of discharge. In both cases, there is an initial instantaneous rise in cell voltage. The magnitude of this step change can, in principle, be used as a basis for estimation of cell resistance. However,



XBL7912-14563

Fig. 2. Dependence of total cell voltage on relaxation time. Simulation parameters as in Fig. 1, except as indicated.

Curve A: $\lambda(t = 0) = 60.8\%$, $R_I = 0.15 \Omega \text{ cm}^2$, $T(t = 0) = 468.2^\circ\text{C}$,
 $T_o(\text{at start of previous discharge}) = 450.0^\circ\text{C}$.

Curve B: $\lambda(t = 0) = 47.9\%$, $R_I = 0.14 \Omega \text{ cm}^2$, $T(t = 0) = 496.2^\circ\text{C}$,
 $T_o(\text{at start of previous discharge}) = 470^\circ\text{C}$.

the numerical predictions cannot be used directly because the effects of double layer capacity are not included in the model, and because the final total cell voltage, prior to interruption, can be much lower than expected in practice, due to the acute nature of the predicted failure mechanism. Therefore, separate calculations are necessary to estimate the interrupter resistance.

At the instant of interruption, there is no change in the composition profile. The potential profile retains the same shape within the negative electrode, and the potential difference $\Phi_1 - \Phi_2$ in the positive is constrained to maintain the same value because of the double layer capacity. Consequently, at any point in the system, Ohm's law gives

$$\frac{i_1}{\sigma} - \frac{i_2}{\kappa} = -\nabla\eta = \frac{i_1^0}{\sigma} - \frac{i_2^0}{\kappa}, \quad (1)$$

where the superscript refers to conditions just before interruption.

Since $i_1 + i_2 = 0$ and $i_1^0 + i_2^0 = I$, one may write

$$i_1 - i_1^0 = -\frac{I\sigma}{\sigma+\kappa}, \quad (2)$$

which indicates that the resistance of matrix and solution are effectively in parallel, even though each segment of the electrode is in series.

Combination of Eq. (2) and Ohm's law for the matrix phase gives the change in cell voltage, $\Delta(V-V^0)$, as

$$\frac{\Delta(V-V^0)}{I} = \int_0^{L_T} \frac{dy}{\sigma+\kappa}, \quad (3)$$

where the left side represents the interrupter resistance, R_I . In the computer calculations, R_I is dominated by the resistance across the separator because the matrix conductivity is assumed to be infinite in the negative and high in the positive electrode. The separator resistance changes only slightly during operation of the cell, in response to variations in electrolyte conductivity.

It should be emphasized that the theoretical models for the LiAl/FeS cell⁶ do not include double layer effects since they are not generally regarded as being significant in the normal operation of a cell. Therefore, for the purpose of measuring the cell polarization characteristics, one may prefer the resistance to be measured after charging of the electric double layer has been completed. For this system, the double layer relaxation time, from point to point within an electrode, is estimated as approximately 50 ms,⁶ whereas relaxation of concentration profiles by diffusion and reaction is on the order of 3000 s (see above).

After interruption, the voltage gradually approaches the equilibrium open circuit cell potential. The shape of the curves is determined by the details of the reactions that occur in the individual electrodes. In particular, a corrosion potential is established in the positive by reactions IIA and IIB. In example A, all the Li_2S has been converted to Li_2FeS_2 after approximately 2450 s, and the voltage rises sharply to the open circuit value, $U_o = 1.34$ V. Curve B does not show this effect because some Li_2S still remains when reactions IIA and IIB are completed. In this case, the voltage slowly approaches the open circuit potential, $U_o - U_{\text{IIA},o} = 1.3074$ V, as the electrolyte composition

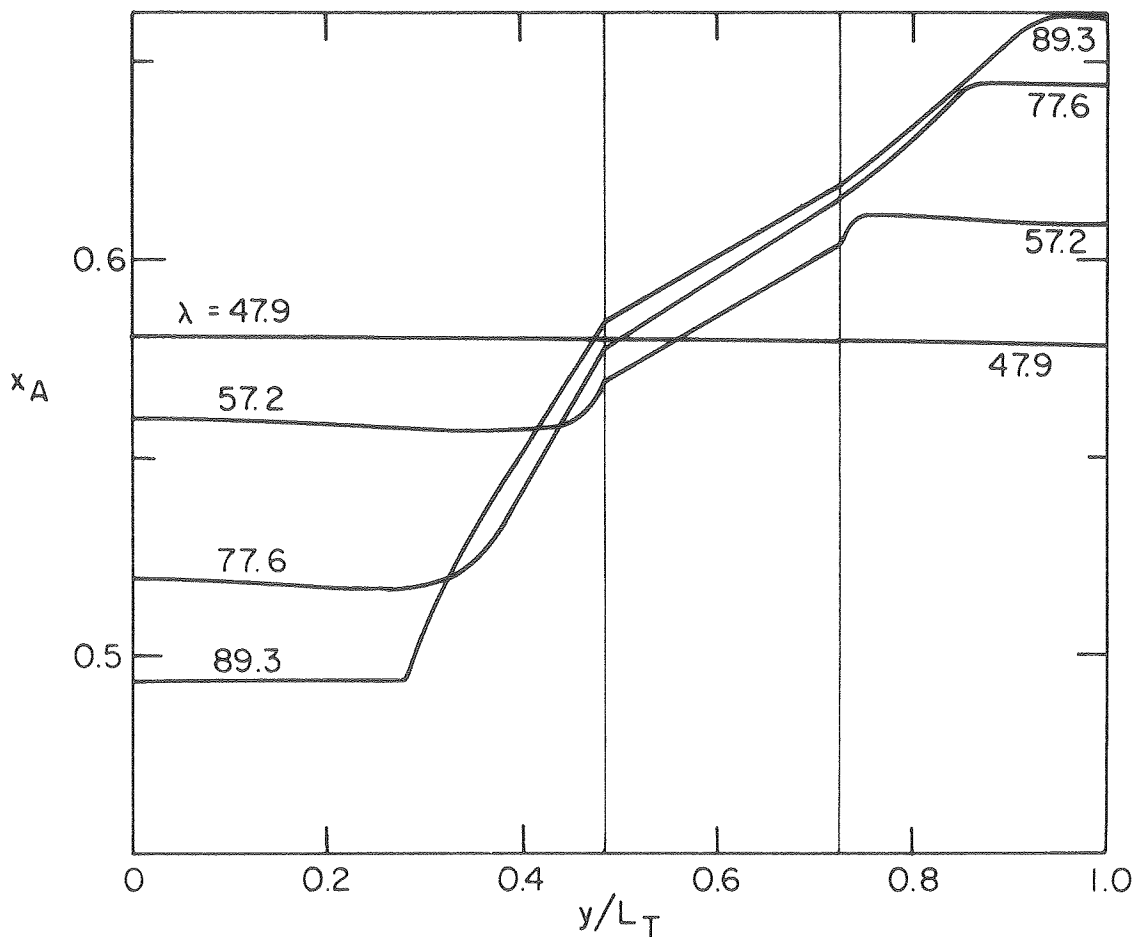
becomes more uniform. It should also be noted that the small initial rate of rise of cell voltage shown in the examples is atypical, and it results from potential drop across the sharp spike of precipitate that was responsible for the rapid decline in cell voltage before current interruption. Both theoretical and experimental results indicate that the initial voltage rise is more rapid when the current is interrupted before the cutoff voltage is reached.⁷

Charging

Figure 3 shows simulated composition profiles at different stages of a constant current charge. A relaxation time of two hours was included between the initial discharge and the start of the charging process. The parameter λ represents the overall state of charge; when the cutoff voltage of 1.65 V is reached, 89.3% of the total theoretical capacity is available for the next discharge.

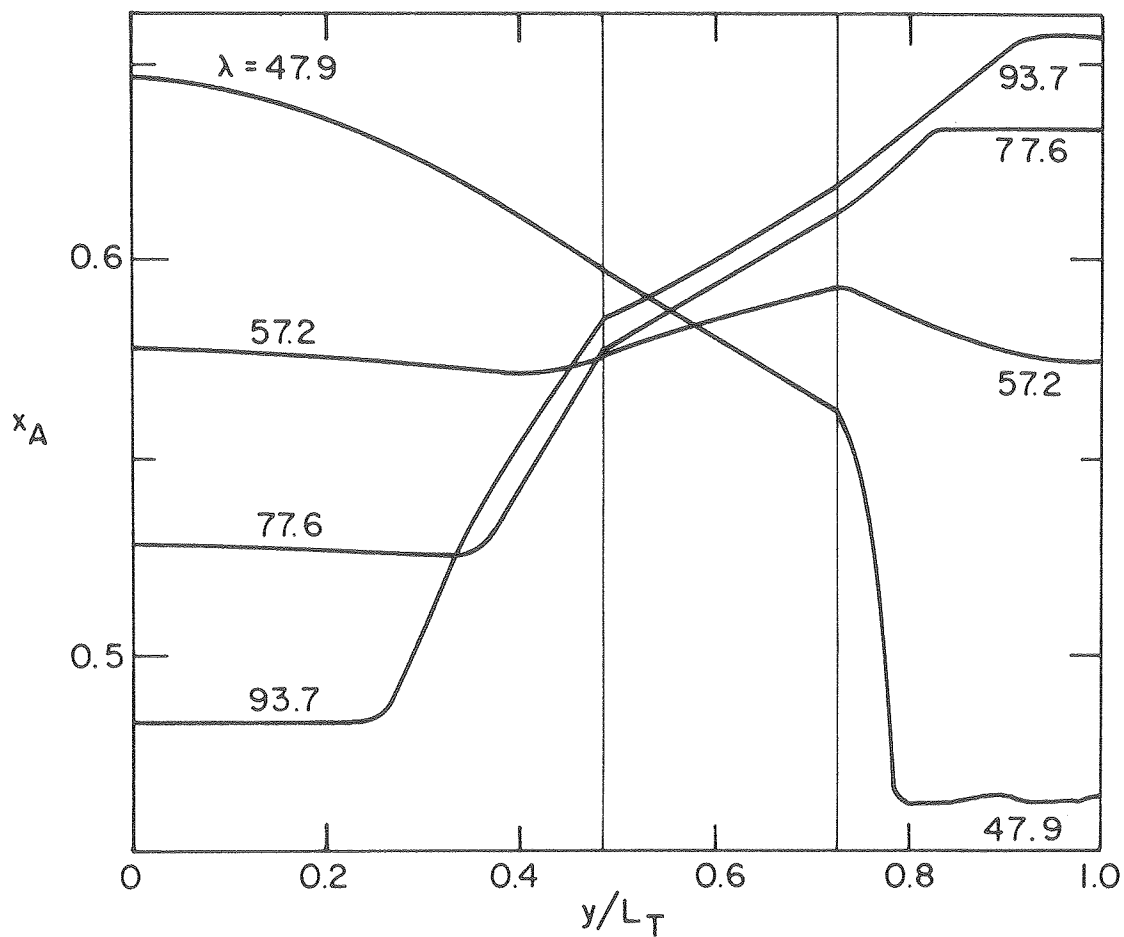
In contrast to discharge, lithium ions are now introduced into the electrolyte at the positive electrode and transported across the separator to the negative electrode, where they are incorporated into the LiAl alloy. The composition profiles represent the combined effects of diffusion, migration, and electrochemical reaction. An almost constant composition gradient is established across the separator, but the electrolyte concentration in the reservoir rises significantly during the charge. The model predicts that the electrolyte composition is almost uniform behind each reaction front.

The variations in electrolyte concentration in Fig. 3 can be compared with those in Fig. 4, for the same cell, but without relaxation



XBL7912-14567

Fig. 3. Position dependence of mole fraction of LiCl at different states of charge for a constant current charge of -41.6 mA/cm^2 . A relaxation time of 2 hours is included between the end of the previous discharge and the beginning of the charging process. Simulation parameters: $T(t = 0) = 480.4^\circ\text{C}$, see also Fig. 1.



XBL 7912-14566

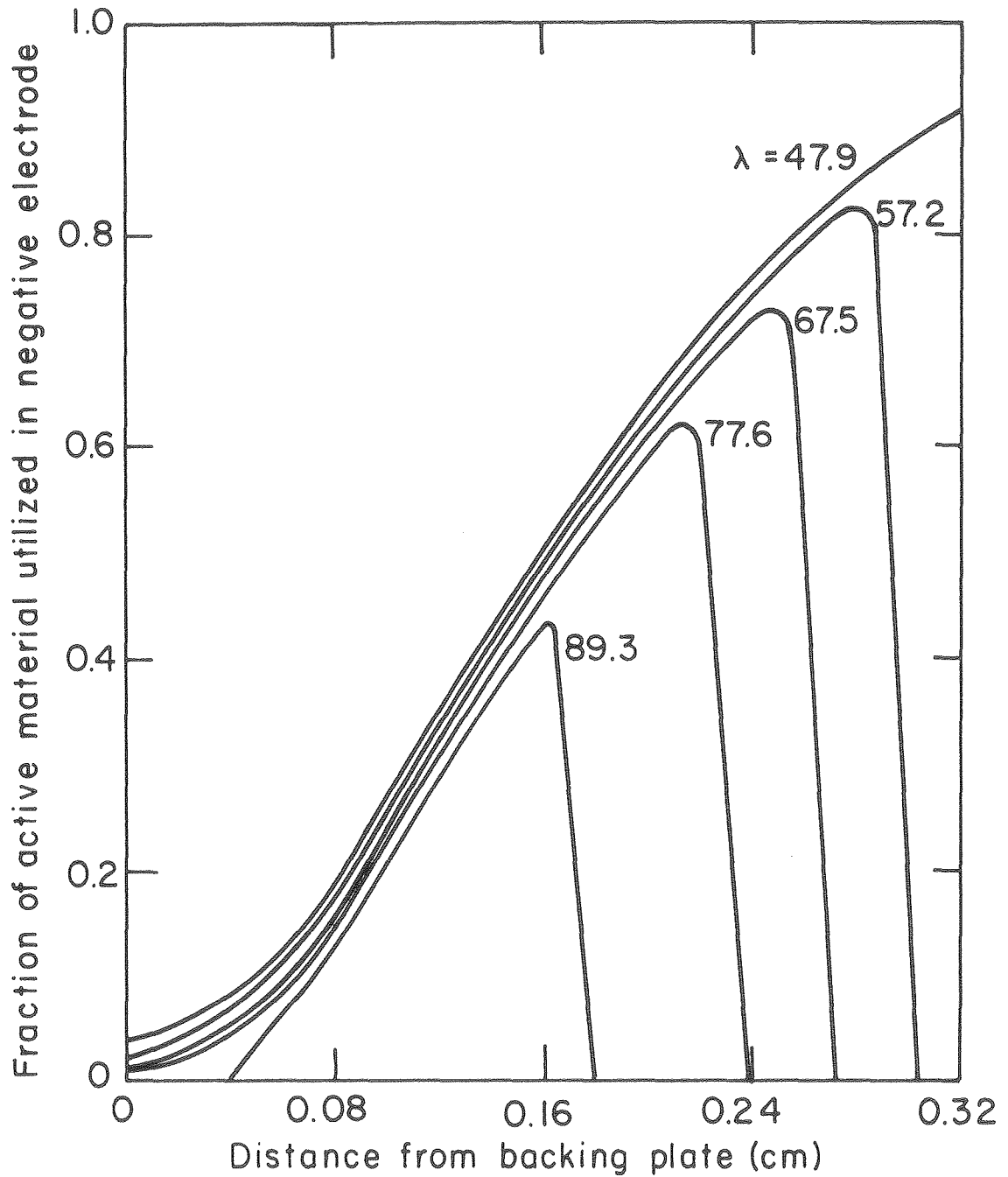
Fig. 4. Position dependence of mole fraction of LiCl at different states of charge for a constant current charge of -41.6 mA/cm^2 . No relaxation between the end of the previous discharge and the start of the charging process. Simulation parameters: $T(t = 0) = 496.2^\circ\text{C}$, see also Fig. 1.

between discharge and charge. At $\lambda = 77.6$, the profiles are very similar in the two cases, and there is little trace of the composition profile before the charge was started.

The average cell temperature in Fig. 3 falls from 753.5 to 740.0 K during the charge, as a result of reversible heat effects and heat transfer to the surroundings. Consequently, the saturation limit for KCl rises, and precipitation begins at the reaction front in the negative electrode when $\lambda = 85.9$. The temperature of the cell in Fig. 4 also falls, but over the range 769.4 to 751.6 K, and precipitation is delayed until $\lambda = 91.1$. For this reason, 93.7% of the theoretical capacity can be recovered before the resistance across the precipitated region becomes excessive and the cutoff voltage is reached.

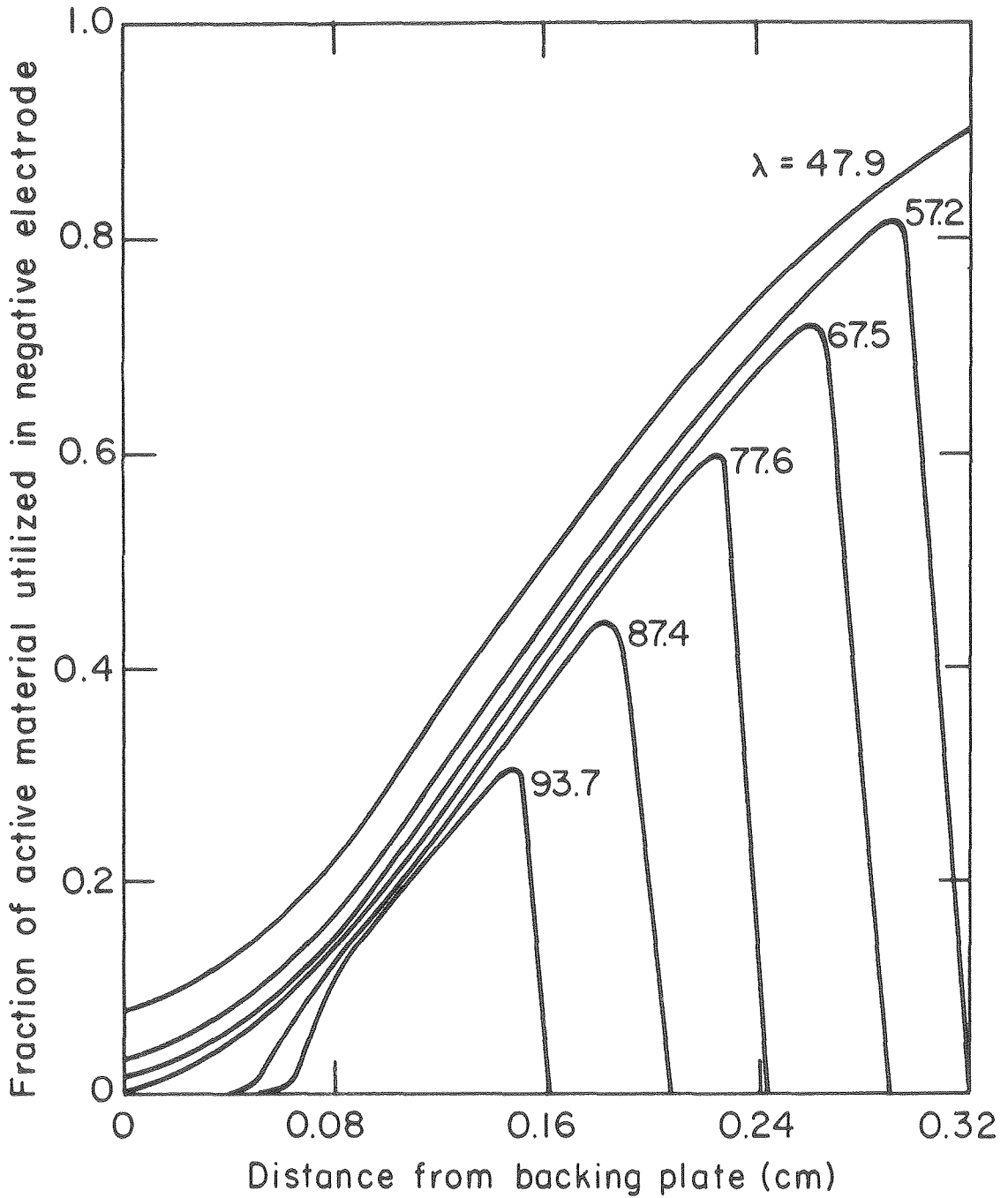
The difference in charging behavior caused by the temperature drop during relaxation emphasizes the need for careful thermal management of battery modules. At lower charging current densities the temperature falls even more dramatically, but the maximum and minimum concentrations are smaller at a given state of charge, and precipitation of KCl no longer controls the final value of λ . For the cell characteristics used in the simulations, a current density of -70 mA/cm^2 is needed to keep the average cell temperature reasonably constant.

Figures 5 and 6 show the fraction of active material utilized within the negative electrode, at several overall states of charge, for the examples in Fig. 3 and Fig. 4, respectively. A comparison of the curves at $\lambda = 47.9$ ($t = 0$), shows the increase in nonuniform utilization of reactants that results from relaxation of the electrolyte composition. The general charging mechanism is similar in two cases: the region closest to the electrode/separator interface is recharged



XBL7912-14565

Fig. 5. Fraction of active material utilized in negative electrode at different overall states of charge during a constant current charge of -41.6 mA/cm^2 . A relaxation time of 2 hours is included between the end of the previous discharge and the beginning of the charging process. Simulation parameters are as in Fig. 1.



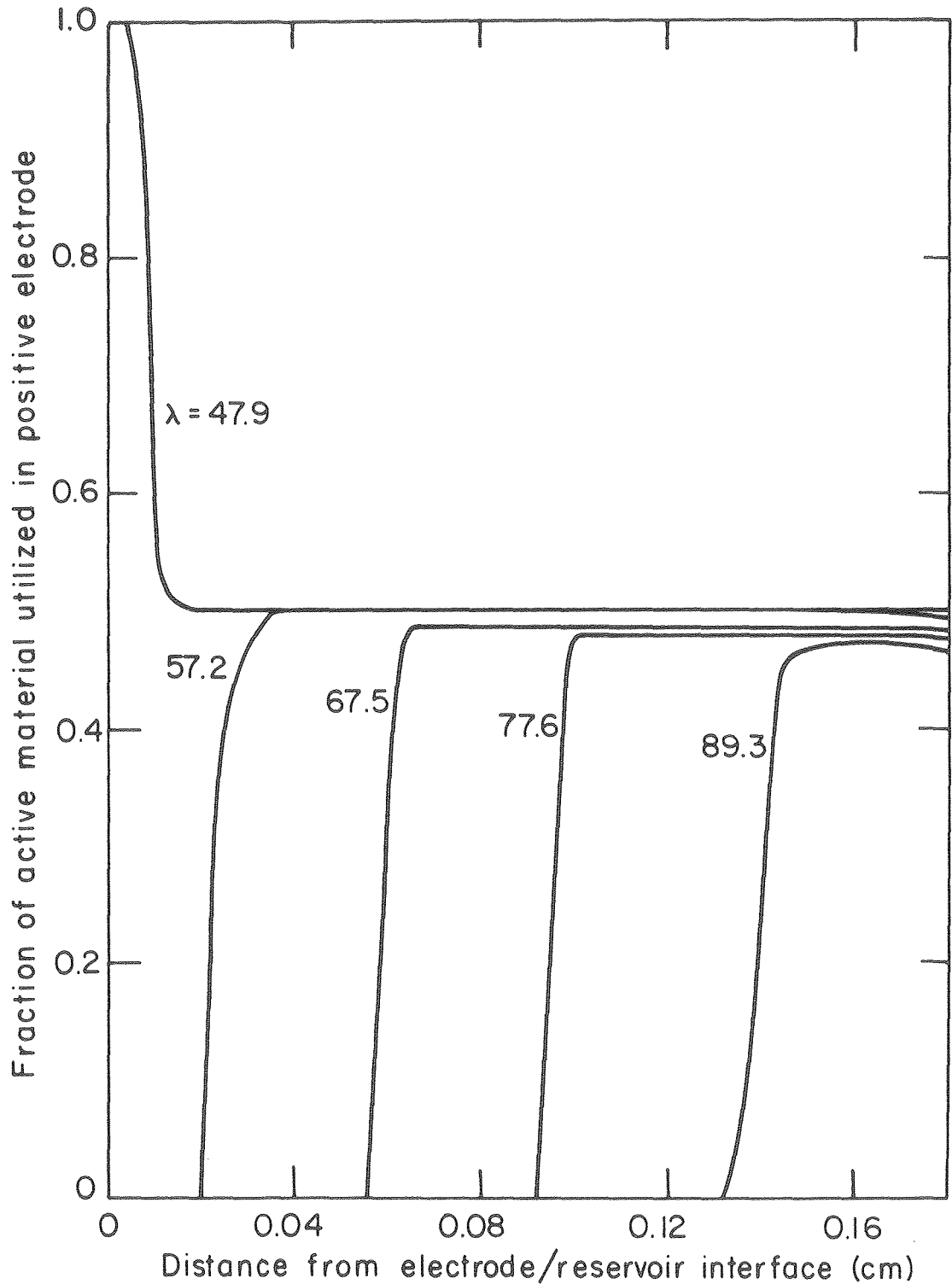
XBL 7912-14564

Fig. 6. Fraction of active material utilized in negative electrode at different overall states of charge during a constant current charge of -41.6 mA/cm^2 . No relaxation between the end of the previous discharge and the start of the charging process. Simulation parameters are as in Fig. 1.

first, and the reaction front moves back through the electrode as the alloy is completely reconverted to β -LiAl. Further reaction of the β -LiAl is not included in the model because the necessary increase in overpotential of almost 0.3 V⁸ cannot be obtained with the specified cutoff voltage. However, recent evidence⁹ suggests that the change in overpotential when a particle becomes completely converted to β -LiAl may not be as dramatic as reported previously.⁸ Consequently, reaction may be possible at the surface of particles where no α -Al remains. In general, diffusion of lithium in the β -phase is considerably faster than in α -Al,¹⁰ and only very small concentration differences are predicted across the outer β -LiAl layer.

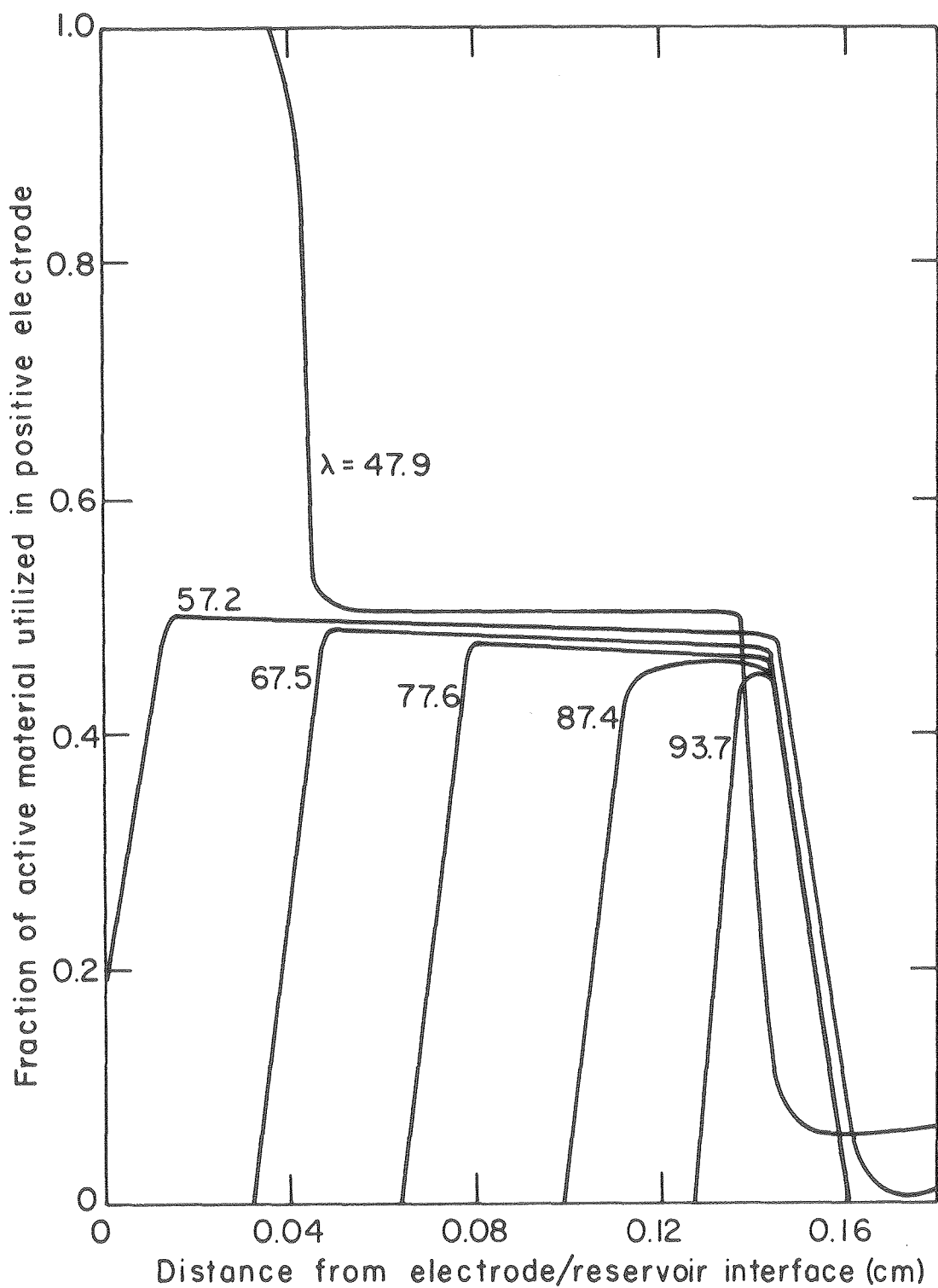
The complementary reaction distributions for the positive electrode are presented in Fig. 7 and Fig. 8. The results at $\lambda = 47.9$ show explicitly the equalization in local state of charge that takes place during relaxation. Figure 7 shows that reaction IIA occurs preferentially at the front of the electrode, adjacent to the reservoir, and that a sharp reaction front moves through the electrode as Li_2FeS_2 is consumed. This mechanism also predominates in Fig. 8, although the final distribution of unreacted material is shifted from the back of the electrode. Figure 8 also indicates that, early in the charge and at a distance of approximately 0.14 cm, FeS reacts cathodically to form X-phase, in accordance with reaction IIA. This self-discharge process corresponds, in part, to the charge equalization predicted during relaxation. The effect is more pronounced at lower current densities.

The variations in total cell voltage for several constant current



XBL7912-14561

Fig. 7. Fraction of active material utilized in positive electrode at different overall states of charge during a constant current charge of -41.6 mA/cm^2 . A relaxation time of 2 hours is included between the end of the previous discharge and the beginning of the charging process. Simulation parameters as in Fig. 1.



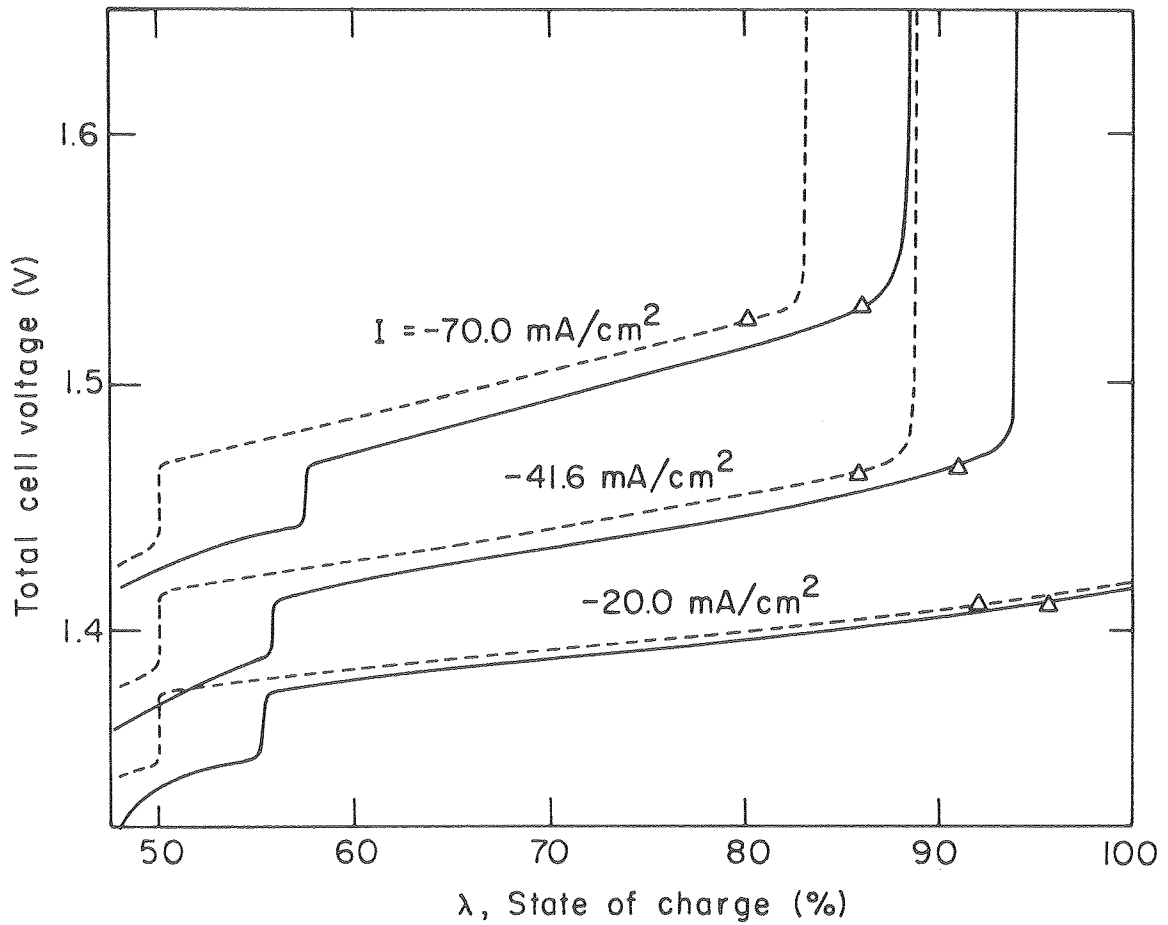
XBL 7912-14562

Fig. 8. Fraction of active material utilized in positive electrode at different overall states of charge during a constant current charge of -41.6 mA/cm^2 . No relaxation between the end of the previous discharge and the start of the charging process. Simulation parameters as in Fig. 1.

charges are presented in Fig. 9. In each case, there is a relatively sharp rise in electrode potential when reaction IIB is completed in the positive electrode because the corrosion potential can no longer be maintained. Also, precipitation of KCl in the negative electrode is predicted, and the local reduction in electrolyte conductivity that results causes a sharp increase in resistance at the higher current densities. At $I = -20 \text{ mA/cm}^2$, charging is completed before precipitation effects dominate. The time for onset of precipitation is sensitive to the cell temperature, and this is largely responsible for the lower final states of charge that are predicted when a period of relaxation is included in the operating cycle.

Experiments on the charging behavior of LiAl/FeS cells⁷ show that the positive electrode current collector potential, measured relative to a reference electrode placed adjacent to the separator, can rise sharply towards the end of charge. The rate of change of this potential can be larger than that of the negative electrode current collector, and this might be interpreted as a positive electrode limitation on charging. There are several possible reasons for this apparent discrepancy between experiment and theory:

- (a) reduction in positive electrode porosity caused by expansion of the negative,
- (b) reduction in available electrode capacity and uncertainty in state of charge,
- (c) development of high matrix resistance in the positive electrode due to poor electrical connectivity of the phases or large



XBL 7912-14578

Fig. 9. Dependence of total cell voltage on state of charge during constant current charges. Simulation parameters as in Fig. 1. and $\lambda(t = 0) = 47.9\%$.

- : charge begins immediately after discharge, $T(t = 0) = 480.4^\circ\text{C}$.
- - - : 2 hours relaxation between discharge and charge, $T(t = 0) = 496.2^\circ\text{C}$.
- Δ : onset of precipitation of KCl in negative electrode.

contact resistances.

Additional experiments may be needed to obtain a clearer picture of the factors that limit the charging behavior and to assess the validity of the numerical predictions. The nature of overcharge reactions, and the potentials at which they become thermodynamically feasible, may also need to be investigated.

Conclusions

A mathematical model of the LiAl/FeS cell has been used to investigate the influence of relaxation on the charging characteristics of the system. The analysis indicates that composition variations become less pronounced during relaxation, but the local state of charge within the electrodes can become more nonuniform. The concentration changes induced on charging mask the effects of current interruption and the effect of relaxation on cell temperature can be more important. The model shows that precipitation of KCl in the negative electrode can cause a rapid rise in applied potential towards the end of charge, but that the effect is not critical at low current densities. The results obtained are sensitive to the details of the heat balance used in the calculation, and this reflects a need for precise thermal management of LiAl/FeS battery modules.

Acknowledgment

The authors are extremely grateful to the members of the Chemical Engineering Division at the Argonne National Laboratory for many useful discussions and valuable suggestions. This work was supported by the Division of Solar, Geothermal, Electric and Storage Systems, Office of the Assistant Secretary of Energy Technology, U. S. Department of Energy, under contract No. W-7405-Eng-48.

Nomenclature

c_i	concentration of species i (mol/cm^3)
D	diffusion coefficient (cm^2/s)
F	Faraday's constant (96487 C/equiv)
h	mesh size (cm)
h_o	heat transfer coefficient ($\text{W}/\text{m}^2 \cdot \text{K}$)
\underline{i}_1	superficial current density in matrix phase (A/cm^2)
\underline{i}_2	superficial current density in pore phase (A/cm^2)
I	superficial current density to an electrode (A/cm^2)
L	thickness of electrode or separator (cm)
L_T	width of cell sandwich (cm)
N	number of LiAl particles per unit electrode volume (cm^{-3})
r_i	inner radius of outer region of β -LiAl in spherical pellet
r_o	radius of particle at solid/electrolyte interface
R_g	grid resistance ($\Omega \text{ cm}^2$)
R_I	interrupter resistance ($\Omega \text{ cm}^2$)
T_o	initial temperature (K)

U_{j_0}	theoretical open-circuit potential for reaction j , relative to a reference electrode of a given kind (V)
V	cell voltage (V)
w	reservoir width (cm)
x_A	mole fraction of LiCl

Greek letters

ϵ	porosity
η	$\phi_1 - \phi_2$
κ	effective solution conductivity (mho/cm)
λ	state of charge (%)
σ	effective matrix conductivity (mho/cm)
ϕ_1	electric potential in the matrix (V)
ϕ_2	electric potential in the electrolyte (V)

Subscripts

lim	limiting value
s	separator
sat	saturation value
β	β -LiAl
+	positive electrode
-	negative electrode

Superscripts

o	initial value
---	---------------

β β-LiAl
- average value

References

1. R. Pollard and J. Newman, submitted to J. Electrochem. Soc.
2. J. S. Dunning, D. N. Bennion, and J. Newman, J. Electrochem. Soc., 120, 1005 (1973).
3. H. Gu, D. N. Bennion, and J. Newman, Ibid., 123, 1364 (1976).
4. R. Pollard, Dissertation, University of California, Berkeley (1980).
5. K. Nisancioglu and J. Newman, J. Electrochem. Soc., 120, 1339 (1973).
6. J. Newman and R. Pollard in "High Performance Batteries for Electric Vehicle Propulsion and Stationary Energy Storage," Progress Report for the Period 4/78-10/79, ANL 79-94, Argonne National Laboratory (November 1979).
7. L. Redey and D. R. Vissers, personal communication.
8. J. R. Selman, D. K. DeNuccio, C. J. Sy, and R. K. Steuneberg, J. Electrochem. Soc., 124, 1160 (1977).
9. C. J. Wen, B. A. Bonkamp, and R. A. Huggins, The Electrochem. Soc. Mtg., Seattle, May 21-26, 1978, Extended Abstract No. 171.
10. C. A. Melendres, J. Electrochem. Soc., 124, 650 (1977).